CHAPTER 5

Cloud radiative smoothing

It was discussed in section 1.3 that horizontal photon transport results in a smoother appearance of the observed nadir radiances at small scales, if compared to the corresponding optical thickness. The horizontal photon transport is the reason for the occurrence of a scale break in power spectra of radiance observations. The term cloud radiative smoothing has been denoted for this effect and refers to small scales only. The results presented in this section are based on different physical processes and reveal that some of these processes exhibit cloud radiative smoothing in large and small scales. Therefore, an explicit differentiation between the effects in different scales is required, and the terms small and large scale cloud radiative smoothing are introduced.

In the following sections, the effects of gas absorption, surface albedo, and two layer clouds on the spectral behaviour of nadir radiances are analysed. The effects are qualitatively identified by the application of the power spectrum analysis (section 1.2) to the radiances. Each of the sections is separated in an experimental and a theoretical part. The experimental part utilises nadir observations taken during the BBC campaign (section 2.2) while the theoretical part verifies the results by utilising RT simulations. Prior to the analysis, the data preprocessing and the set up for the RT simulations is discussed. The outcome of the experimental analysis resulted in two publications: *Schröder and Bennartz* (2003) and *Schröder et al.* (2004). The following sections reproduce the results of these publications. In fact, all figures related to observations are taken from *Schröder et al.* (2004).

5.1. Data preprocessing and choice of parameters

The spectrometric data was recorded during the Baltex Bridge Cloud (BBC) campaign in The Netherlands in September 2001. During the campaign coordinated observations of clouds were carried out with groundbased and airborne instruments. The Freie Universität Berlin participated with its airborne research platform, a Cessna 207T. The Cessna was equipped with a compact compact airborne spectrographic imager (*casi*) and the Free University Berlin's Integrated Spectrographic System (FUBISS), see sections 2.1.1 and 2.1.2, respectively. In total 59 flights were conducted with the Cessna 207T, with leg lengths varying between 10 km and 76 km. Various broken, closed and multi-layer clouds were observed.

It is essential for a reliable power spectrum analysis, that the data sets have a certain degree of similarity. That means that the observed radiances should depend on similar physical processes, e.g. the reflection of solar radiation by clouds only. Therefore, flight legs were selected that fulfill the following four criteria: 1) a cloud fraction of approximately 100%, 2) no altostratus, 3) a cirrus coverage smaller than 1/8, 4) a minimum leg length of 40 km. The leg length is calculated from the product of the ground speed and the duration since leg start, the cloud fraction is determined as discussed in section 2.3 and criteria 2) and 3) are verified using the flight protocol. Only five legs meet all four criteria. A detailed description of these flight legs is given in Table 5.1 and Figure 2.5. During the flights on 06 September 2001 (leg 4) and 20 September 2001 (legs 2 and 3) single layer clouds were observed. On 06 September 2001 (leg 5) and 23 September 2001 (leg 2) the radiances were recorded over two layer cloud systems, with the upper layer being broken in both cases. The impact of two layer cloud systems on cloud radiative smoothing is investigated with the help of *casi* data, since FUBISS was not operating on 06 September 2001. *Casi*'s nadir

TABLE 5.1. Description of flight missions that are used to study cloud radiative smoothing.

Date	Leg	Start time [UTC]	Stop time [UTC]	Leg length [km]
06 September 2001	4	10:21	10:33	45
06 September 2001	5	10:35	10:55	65
20 September 2001	2	12:28	12:52	46 (*casi*), 68 (FUBISS)
20 September 2001	3	12:57	13:13	68
23 September 2001	2	13:13	13:32	65

radiance at 620 nm is used to minimise the impact of large surface albedos. The study of the impact of absorption and surface albedo on cloud radiative smoothing is based on data measured on 20 September 2001 (leg 2). The radiance measurements are taken from FUBISS *vis* since its signal-noise-ratio (SNR) is more than an order of magnitude larger than *casi*'s SNR (see section 2.1). The other two single layer cloud cases are not studied because the range of the small scales is too short for a reliable interpolation (flights in the direction of the wind). The investigation is carried out in a wavelength range between 850 and 950 nm to have the greatest possible variety of absorption intensities. The restriction to wavelengths smaller than 950 nm is due to a rapid decrease of FUBISS's SNR towards 1000 nm (see Figure 2.4). The sampling rate of *casi* is 112 ms while FUBISS measures every 750 ms with an integration time of around 50 ms. In combination with the ground speed of the aircraft (50 m s^{-1}), spatial sampling rates of 6 m and 40 m are calculated for *casi* and FUBISS, respectively.

The RT simulations are performed with the *local estimate model* presented in section 4. The input parameters for the simulations are generated on the basis of surrogate cloud fields (see section 3.2) combined with the microphysical model presented in section 3.4. Using the cloud top and cloud base height from the surrogate cloud field, the microphysical model enables the computation of w_0, σ_{ext}, and $\tilde{\beta}$ at every grid box. A condensation rate of c_w=1.5x10^{-3} g cm^{-4} and a droplet number concentration of N=200 cm^{-3} is chosen. The value of c_w is determined using the observations of *Meywerk et al.* (2002) and is almost constant with maximum variations of 2%. N=200 cm^{-3} is a typical value for a medium polluted air mass (*Brenguier et al.*, 2000). To reduce the computational effort, the input parameters are averaged in the vertical dimension. A constant cloud top at 1 km and a geometrical thickness of 0.2 km is chosen. The average optical thickness of a single cloud layer is 8.2, which translates to a mean free photon path of $1/\langle\tau\rangle \,\mathrm{x}\, 0.2$ km=0.024 km. This plus the smallest resolution of the observations resulted in choosing a box size of 10 m. To get coincidence with the mean leg length of the observations, a total amount of 4096 boxes is utilised. A sun zenith angle of 38.6° is used which corresponds to the situation on 20 September 2001 (leg 2).

The surrogate cloud fields are simulated with fixed vertical box sizes of 2 m and for 4096 boxes in the horizontal dimension. In order to generate the surrogate cloud field the slopes of the power spectra and the standard deviations of the histograms of the cloud top height and the geometrical thickness H are used as input. The histograms are assumed to be Gaussian like. The slopes of both parameters is set to 5/3 (see also section 1.2) while the standard deviations are 23 and 52 m in case of cloud top height and H, respectively. The standard deviations are retrieved based on the results of *Meywerk et al.* (2002) but rescaled to lower values. However, both values, the standard deviation and the slope of the cloud top height, are in close agreement with the findings of *Fischer et al.* (1991). The scaling is related to a reduction of the mean optical thickness to reduce the computational effort. Due to similar reasons, the Henyey-Greenstein function with an asymmetry factor of 0.81 is utilised (see section 4.3 for a discussion of both aspects). After application of

the microphysical model and execution of the vertical averaging, the slope of the optical thickness is 1.75.

It should be mentioned that a slope of 5/3, constant over all scales considered in this study, may not be an appropriate value for H or LWP. In literature, several investigations of the spectral behaviour of LWC are found (e.g. *Davis et al.*, 1996 and *Davis et al.*, 1999) while the power spectral behaviour of LWP has not been intensively studied so far. LWP data sets from the BBC campaign (*Crewell et al.*, 2004) are subjected to the power spectrum analysis. In total 4 subsets of LWP are investigated, each having at least 95% of the data points larger than 0.15 g m^{-2}. The mean (small scale) slope is roughly 8/3. A scale break is found at ~860 m for LWP data from 23 September 2001, while the power spectrum based on data from 05 September 2001 exhibits no scale break. If the threshold is neglected and the complete set from 23 September 2001 is considered, the large scale slope is slightly larger than 1.4. These results stand in contrast to those of *Wood and Taylor* (2001): They found a slope of 1.51 ± 0.06 for measurements over open oceans and no scale break.

Further on, the investigation of cloud geometries, based on data from *Meywerk et al.* (2002), revealed that the standard deviation of cloud base height (61 m) is significantly larger than for cloud top height (47 m). The cloud base strongly depends on local thermodynamic parameters (section 3.5), while the ascent of cloud top parts is suppressed, if a strong inversion exists. Qualitatively a similar outcome is found in cloud fields simulated with the LES model (see Figure 3.2). Usually cloud base variations are assumed to be small and/or neglected in many investigations related to 3d RT in cloudy atmospheres. The assumption that the cloud base does not vary significantly may not be appropriate but the effect of a variable cloud base on radiance observations has not been addressed so far.

5.2. Surface albedo effects

The reflectance of vegetation is characterised by a strong increase with increasing wavelength around the so-called red edge. The transition between small (~0.1) and large reflectances (~0.5) is centred at around 700 nm and depends on the type of vegetation. The strength of the step can reach 50%. In general, the increase is more pronounced for trees than for grass. The reflectance of soil is in the majority of cases smaller in strength and less steep (*Bowker et al.*, 1985 and *Clark et al.*, 1993). To characterise the impact of the surface albedo on cloud radiative smoothing, nadir radiances measured with FUBISS are utilised. In total, 19 absorption free channels between 660 and 785 nm are used to study this impact. The measurements were taken between 12:28 and 12:52 UTC on 20 September 2001 (leg2). During the measurements the solar zenith angle varied by 1.2° with a mean of approximately 38°.

Figure 5.1 presents an exemplary power spectrum of normalised nadir radiances at 620 and 780 nm. The original power spectrum of nadir radiances at 620 nm is indicated by dots while the corresponding result at 780 nm is not shown for clarity reasons. The squares give the octave binned power spectrum and the solid lines the least square fit to the binned data. The triangles and the dashed lines refer to the power spectrum of nadir radiances at 780 nm. Obviously, the large scale fit of the power spectrum at 780 nm is characterised by a smaller slope than the fit of the power spectrum at 620 nm. This example of the effect of different surface albedos on power spectrum analysis is extended to a larger variety of surface albedos by investigating the spectral behaviour at several wavelengths centred around the red edge.

The results are given in Figure 5.2. It shows the scale break and the large and small scale slope versus wavelength (left panel) and versus reflectance (right panel). The mean reflectance associated with large surface albedos is around 0.51 while the mean reflectance for wavelengths smaller than 700 nm is 0.46. Channels with significant absorption features of O_2 and H_2O are excluded, which explains the gaps in the left panels of Figure 5.2. A typical small scale slope of 3.00 ± 0.05 is found which exhibits no dependence on surface albedo. The scale break and the large scale slope are affected by a variable surface albedo.

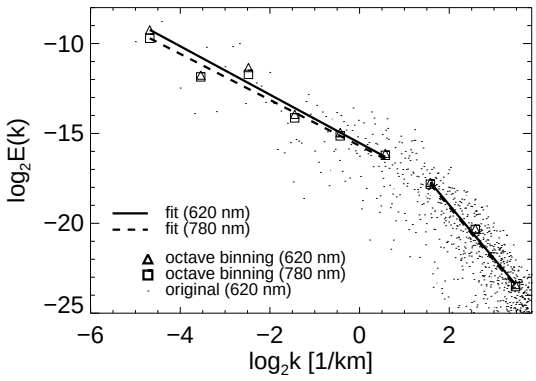

FIGURE 5.1. Power spectrum analysis of normalised nadir radiances recorded on 20 September 2001 (leg 2). The dots present the original result of the power spectrum of nadir radiances at 620 nm while the squares give the corresponding (octave) binned power spectrum. The solid line is the least square fit of the binned power spectrum of radiances at 620 nm. The triangles and the dashed line refer to the power spectrum of nadir radiances at 780 nm. The original power spectrum of nadir radiances at 780 nm is not shown in order to maintain clarity.

The step function nature of the reflectance of vegetation becomes obvious: The transitions between large and small values are found, where a strong change in the reflectance of surfaces covered with vegetation is located spectrally. A large scale slope of 1.34 $\pm$ 0.02 is found for wavelength around 680 nm while the large scale slope around 780 nm is significantly smaller (1.28 $\pm$ 0.02). The scale break at low surface albedos is 344 $\pm$ 22 m and increases to 354 $\pm$ 26 m at large surface albedos. The uncertainties are determined as discussed in section 3. Here, the uncertainty estimation is based on 8 channels around 675 nm and on 5 around 780 nm. The outcome of this estimation reveals that only the effect in the large scales is statistically significant. The results of the small scale slope and the scale break are not significant because they are within the overlap of their standard deviations. Since the scale break is calculated by the interception of the linear interpolations in the small and large scales, the decrease of the large scale slope with increasing albedo translates into the step-like appearance of the scale break.

The increasing surface albedo results in a decrease of the large scale slopes. In the presence of large surface albedos, optically thin parts of the cloud appear brighter while optically thick parts remain almost unchanged. Figure 5.3 proves this statement. It shows the normalised reflectance of the absorption-free channels at 620 and 780 nm, the difference between the normalised reflectances in percent and the corresponding scatterplot. The reflectances were recorded between 12:28 and 12:36 UTC on 20 September 2001 (leg 2), and the normalisation is based on the maximum of each time series. If the cloud surface interaction can be neglected and if a homogeneous cloud is observed, both channels theoretically exhibit a constant bias due to different scattering intensities: the volume extinction coefficients at 620 and 780 nm are 33.7 and 32.2 m^{-1}, respectively, if r_{eff}=10 μm and a size distribution following *Brenguier et al.* (2000) and *Schüller et al.* (2003) is assumed. The asymmetry factor varies by approximately 1%. If inhomogeneous clouds are observed, the cloud microphysical properties can change on spatial scales: If r_{eff} would equal 15 μm instead of 10 μm, the difference between σ_{ext}(620 nm) and σ_{ext}(780 nm) changes from +4.3% to -4.3%.

However, the surface albedo is the major reason for the observed differences between the normalised reflectance at 620 and 780 nm: A maximum difference of more than 25%

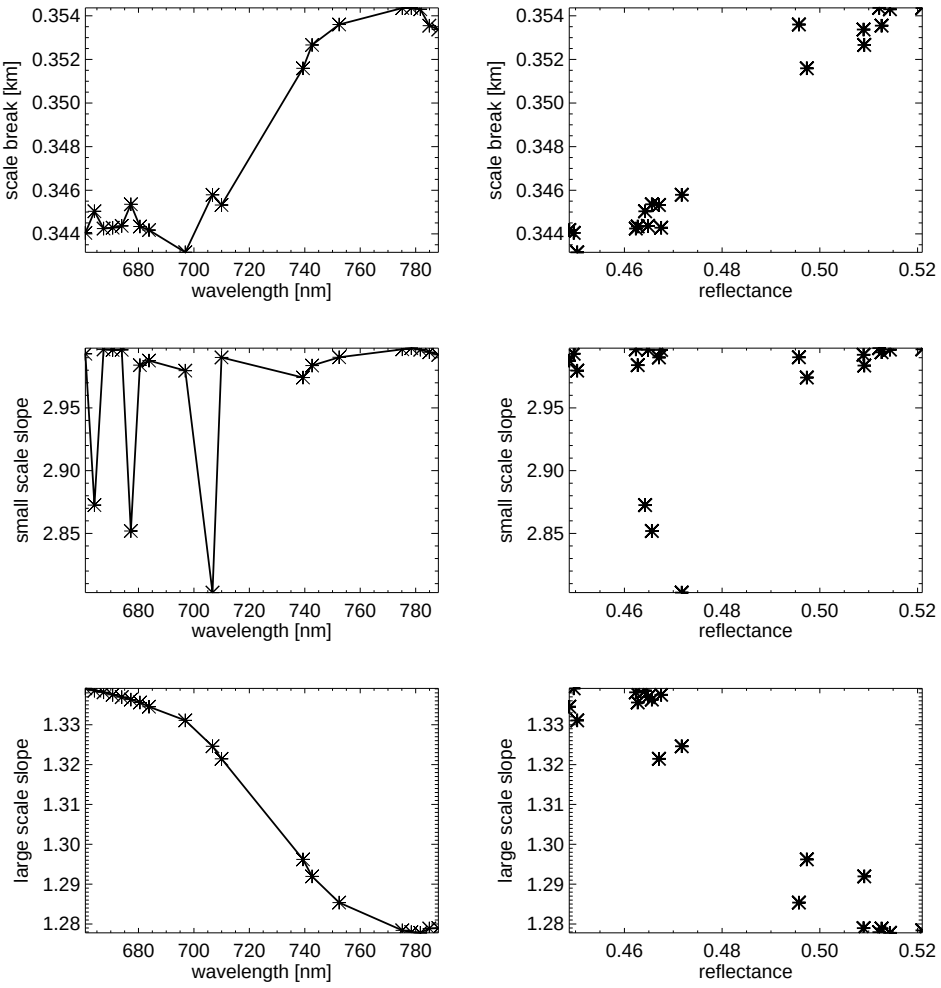

FIGURE 5.2. Scale breaks (upper panels), small scale slopes (middle panels) and large scale slopes (lower panels) versus wavelength (left panels) and versus flight leg averages of observed reflectance (right panels). The data was recorded on 20 September 2001 (leg 2).

is found, and the scatterplot shows a transition to larger normalised reflectances at 780 nm if the normalised reflectance values decrease (Fig. 5.3). The surface albedo brightens optically thin cloud parts (small element numbers, small normalised reflectances) and leaves optically thick parts almost unchanged (large element numbers, large normalised reflectances). In this way spectral power is removed in scales which depend on the cloud morphology. Thicker cloud parts associated with updraft regions and thinner cloud parts where downdrafts are effective divide the cloud field in optically thicker and thinner parts. The size of the cloud cells define the scale where the smoothing can be found in the power spectrum. *Boers et al.* (1988) found a typical cloud diameter of 3-5 km for marine stratocumulus clouds. In addition, large surface albedos lead to an increase of horizontal photon diffusion proportional to the cloud height. The observed mean cloud base height at Cabauw between 12:00 and 13:30 UTC is 1350 m (retrieval described by *Meywerk et al.*, 2002). Both, the mean cloud base height and the typical cloud diameter support our result that large surface albedos affect the large scales only. The term large scale cloud radiative

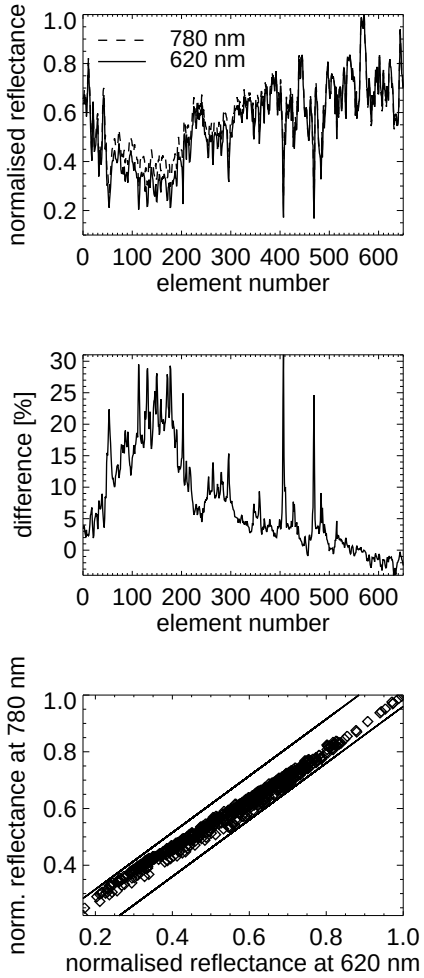

FIGURE 5.3. Normalised reflectance at 620 and 780 nm, their differences in percent as a function of element number and the corresponding scatterplot with limiting lines. The normalisation is based on the maximum of the reflectance at each wavelength. The maximum and minimum radiance values are 248 W $m^{-2}sr^{-1}\mu m^{-1}$ (780 nm) and 320 W $m^{-2}sr^{-1}\mu m^{-1}$ (620 nm) and 55 W $m^{-2}sr^{-1}\mu m^{-1}$ (780 nm) and 54 W $m^{-2}sr^{-1}\mu m^{-1}$ (620 nm), respectively. The data was recorded on 20 September 2001 (leg 2).

smoothing is introduced here. It is an expression for the effect mentioned above, the decrease of the large scale slope, here as a consequence of an increase of the surface albedo. The term large scale cloud radiative smoothing is an extension to previous notations, where cloud radiative smoothing describes the impact of horizontal photon transport on radiation fields, which is effective in small scales only (see section 1.3). The small scale slopes are not affected by the surface albedo because the small scale radiative smoothing depends on scattering of photons within the cloud and not on scattering between the cloud and the surface (see also next section).

An exact knowledge of the spectral albedo is required for the interpretation of nadir radiation measurements (*Wendisch and Mayer*, 2003). Here, it is not possible to quantify the impact of a variable surface albedo, as it was not observed for this leg. Nadir radiance

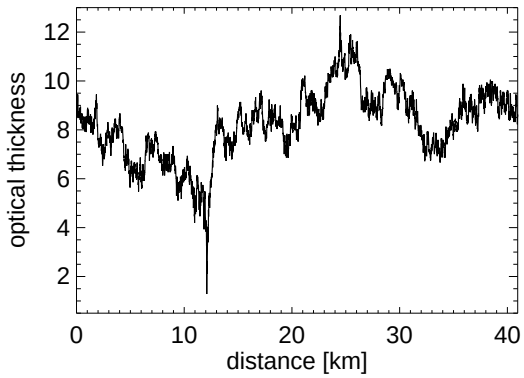

FIGURE 5.4. Optical thickness versus distance. The optical thickness represents the input field for RT simulations.

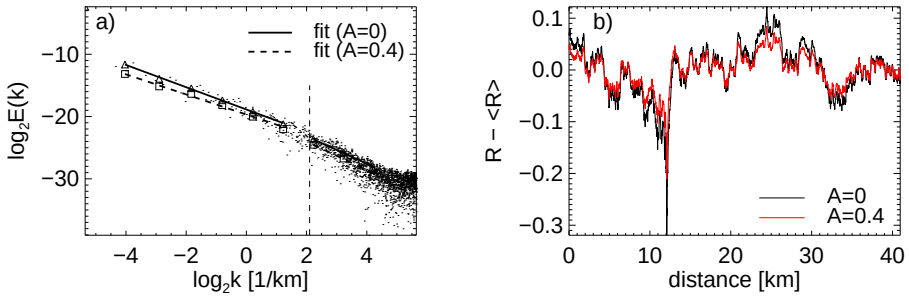

FIGURE 5.5. Power spectra for simulated reflectances with A=0 and 0.4 (Fig. a). The dashed vertical line indicates the scale break. The slopes are given in the text. In Fig. b the mean free reflectance is plotted versus distance.

measurements conducted in clear sky conditions during the BBC campaign exhibit an extremely inhomogeneous surface reflectance in neighbouring areas. This inhomogeneity can influence the absolute values of the slope, but the general effect of the red edge on radiative smoothing probably remains for a large variety of cases.

The presented effect of surface albedo on cloud radiative smoothing is verified by two RT simulations, one having a surface albedo of A=0 and the other of A=0.4. The latter corresponds to maximum values measured during the BBC campaign (*Wendisch et al.*, 2004), and therefore, the verification is carried out for two extreme situations as they might have been observed during the measurements. The optical thickness, which presents the input for both RT simulations, is given in Figure 5.4. The mean optical thickness is 8.2 with a standard deviation of 1.4. The amount of photons per box is $4\text{x}10^7$ and certainly sufficient for studying large scale cloud radiative smoothing.

The spectral behaviour of the simulated reflectances for A=0 and 0.4 and a comparison of the mean free reflectances are shown in Figure 5.5. The large scale slope for the A=0 case, $\beta_l\,(A=0)$=1.79 $\pm$ 0.03 is significantly larger than $\beta_l\,(A=0.4)$=1.61 $\pm$ 0.05, while the small scale slope and the scale break are unaffected by an increase of the surface albedo. Therefore, the qualitative verification is successful but the absolute values of the large scale slopes and the strength of the effect are not in close agreement. The absolute values probably differ due to different statistics of the optical thickness and cloud top height of the artificial and observed cloud while the difference between large scale slopes at high and low

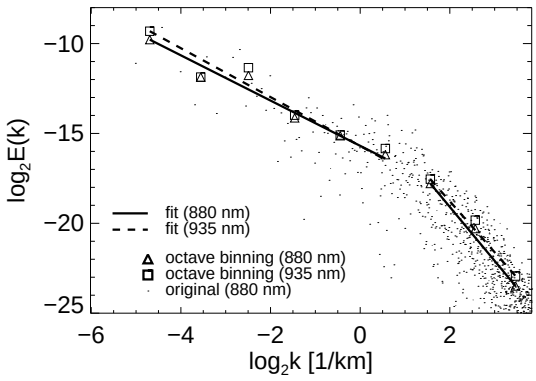

FIGURE 5.6. Power spectrum analysis of normalised nadir radiances recorded on 20 September 2001 (leg 2). The dots present the original result of the power spectrum of nadir radiances at 880 nm while the squares give the corresponding (octave) binned power spectrum. The solid line is the least square fit of the binned power spectrum of radiances at 880 nm. The triangles and the dashed line refer to the power spectrum of nadir radiances at 935 nm. The original power spectrum of nadir radiances at 935 nm is not shown in order to maintain clarity.

surface albedos is due to differences of the surface albedo defined for the simulation and given during the measurements: The larger the surface albedo, the stronger is the large scale cloud radiative smoothing (Fig. 5.2). The simulated case represents an upper boundary of the observable effect on large scale cloud radiative smoothing. One should keep in mind the large spatial variability of the surface albedo (see *Wendisch et al.*, 2004 for a discussion): A=0.4 is within the observed values but is certainly higher than the average surface albedo during the measurements.

5.3. Impact of gas absorption: large and small scale cloud radiative smoothing

The impact of gas absorption on cloud radiative smoothing is investigated using the $\rho\sigma\tau$-water vapour absorption band. FUBISS measurements in the spectral range from 850 to 950 nm (31 channels) are utilised. Except for the different spectral range, the measurements and the evaluation procedures are identical to those in section 5.2.

In Figure 5.6 the original power spectrum of the normalised nadir radiance at 880 nm is shown together with the corresponding octave binned power spectrum (squares) and least square fits to the binned spectrum (solid lines). Except for the original power spectrum, corresponding results (triangles and dashed lines, respectively) are given for normalised radiances at 935 nm. The strong absorption at 935 nm increases the large scale slope and decreases the small scale slope. This analysis is extended to all wavelengths between 850 and 950 nm and summarised in Figure 5.7. The figure presents the scale break and the large and small scale slope versus wavelength (left panels) and versus reflectance (right panels). The overall shape of the water vapour absorption band is obvious in all figures, and the correlation between reflectance and all three parameters is obvious. Reflectance values of 0.53 and 0.28 are observed at 870 and 940 nm, respectively. With increasing absorption the scale break and the small scale slope decrease: the scale break from 355 ± 17 m to 305 ± 26 m and the slope from 3.00 ± 0.03 to 2.83 ± 0.05, each value given at 870 and 940 nm, respectively. The large scale slope increases by about 8% from 1.26 ± 0.02 at 870 nm to 1.36 ± 0.03 at 940 nm.

The uncertainties given above are estimated by subsetting the spectral power (see section 1.2). The uncertainty estimation is based on 11 channels around 870 nm and on 5

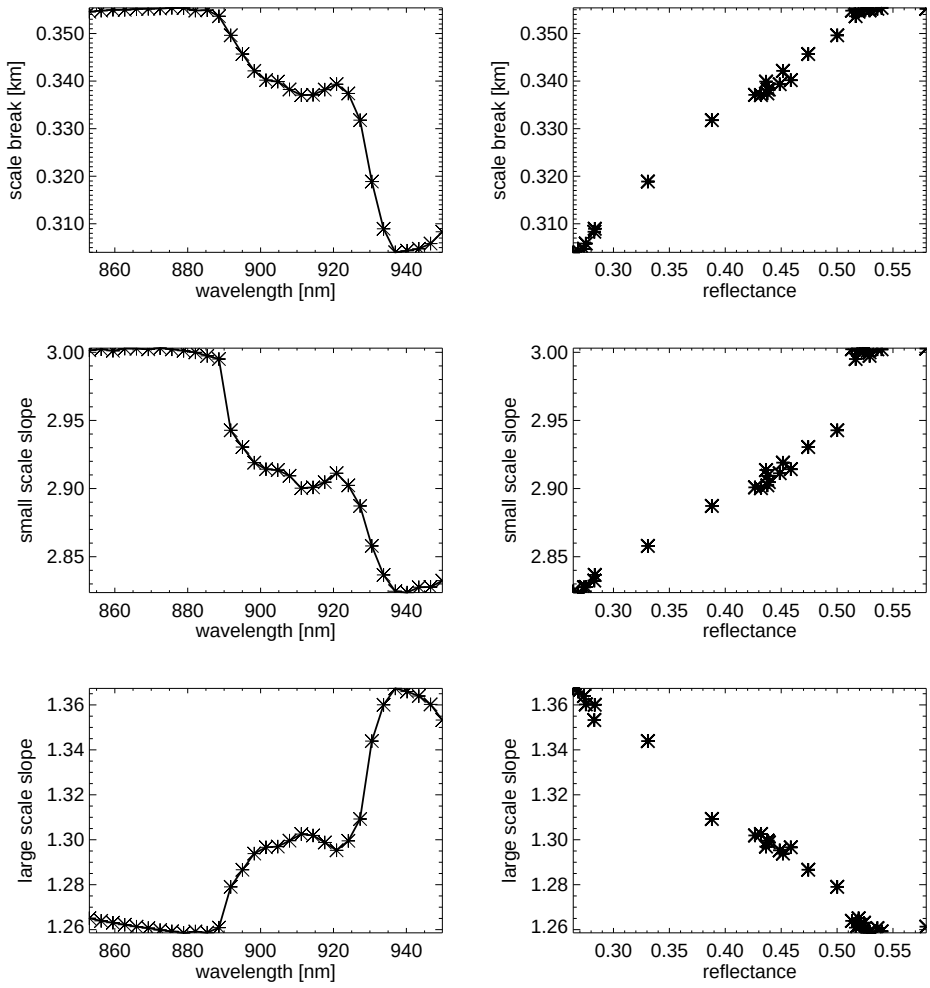

FIGURE 5.7. Scale breaks (upper panels), small scale slopes (middle panels) and large scale slopes (lower panels) versus wavelength (left panels) and versus flight leg averages of observed reflectance (right panels). The data was recorded on 20 September 2001 (leg 2).

around 940 nm. The large and small scale slopes as well as the scale break at large and small reflectance values, are well separated. To give an example: The large scale slope of the absorbing and non-absorbing case is separated by two times the sum of the standard deviations which translates to a 95% confidence of a statistically significant separation. The results for the small scale slope and the scale break indicate a decreasing intensity of cloud radiative smoothing at small scales (see section 1.3). Here, the large small scale slope and the occurrence of a scale break are identified as small scale cloud radiative smoothing. In this way, it is emphasised that cloud radiative smoothing must not necessarily affect the small scales only (see also section 1.2).

If absorption is present, the mean free photon path and, therefore, the likelihood of horizontal photon transport decreases. The stronger the absorption the more the nadir radiance is correlated with the optical thickness field. High frequencies become present again, and the small scale slope decreases. A decreasing mean free photon path lowers the likelihood of photons to travel large geometrical distances within the cloud, which explains the decrease of the scale break. In order to study the effect of larger absorption intensities,

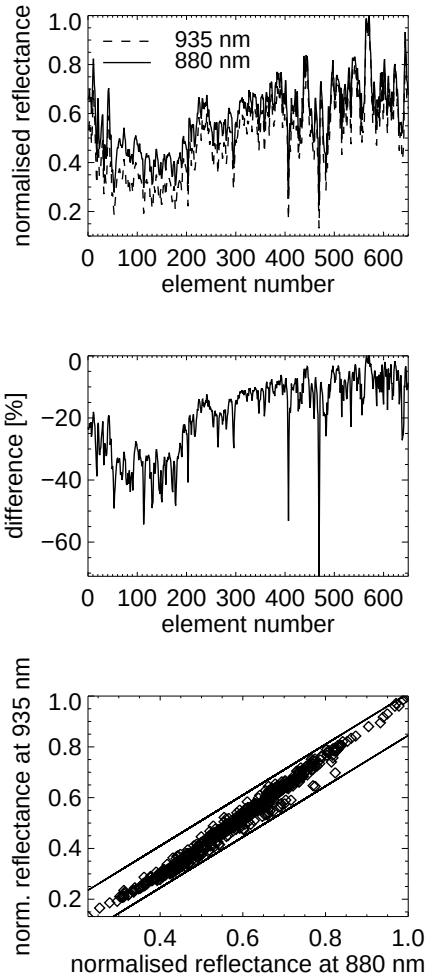

FIGURE 5.8. Normalised reflectance at 880 and 935 nm, their difference in percent as a function of element number and the corresponding scatterplot with limiting lines. The normalisation is based on the maximum of the reflectance at each wavelength. The maximum and minimum radiance values are 145 W $m^{-2}sr^{-1}\mu m^{-1}$ (935 nm) and 274 W $m^{-2}sr^{-1}\mu m^{-1}$ (880 nm) and 4 W $m^{-2}sr^{-1}\mu m^{-1}$ (935 nm) and 18 W $m^{-2}sr^{-1}\mu m^{-1}$ (880 nm), respectively. The data was recorded on 20 September 2001 (leg 2).

spectrally higher resolved observations are required. The scale break should disappear in the high absorption limit. These discussions cannot explain the effect of large absorption intensities on large scale cloud radiative smoothing. In section 5.2 it was demonstrated that large surface albedos are associated with small large scale slopes due to large scale cloud radiative smoothing. Between 850 and 950 nm, the surface albedo of land surfaces is generally large which can be seen at the small large scale slopes for wavelengths around 870 nm (see also previous section). In the case of large absorption, the cloud-surface interaction is reduced. This reduction prevents large scale cloud radiative smoothing and results in increased large scale slopes with increased absorption intensities. In a way, the absorption reverts the impact of the surface albedo, which can be seen if Figures 5.2 and 5.7 are compared.

Figure 5.8 provides an explanation for the impact of high absorption intensities. The figure is similar to Figure 5.3 except that the radiances at 880 and 935 nm are utilised. The asymmetry factor at both wavelengths differs by less than 1%. The volume scattering coefficients at 880 and 935 nm are 32.2 and 34.3 m^{-1}, respectively. Scattering dependencies are a minor process since the transmission intensities at these wavelengths differ by approximately 75%. At 935 nm the large absorption intensity reduces the impact of large surface albedos which becomes evident especially at small element numbers in the middle panel and at small normalised reflectances in the scatterplot: The minima of the radiance at 935 nm are more intense than at 880 nm because the water vapour absorption annihilates the surface albedo impact in cases of relatively thin clouds. In the scatterplot this becomes evident in the shift to lower normalised reflectances. This results in an apparent increase of the contrast of the radiance at 935 nm compared to the radiance at 880 nm, which explains the increase of the large scale slope.

Even though the physical explanation of the findings sounds reasonable and the uncertainty estimates proof statistical significance, the following problem can arise: The SNR of FUBISS drops rapidly for wavelengths larger than 850 nm, as can be see in Figure 2.4. In addition, the leg averaged signal decreases with increasing absorption. The combination of the leg averaged signal and the sharply decreasing SNR can increase the noise level of the data for increasing wavelengths. This noise might produce enough spectral power in the small scales to give reason for an instrument based small scale slope behaviour similar to that in Figure 5.7. To demonstrate that the noise is not the reason for the results presented in this section, a new spectral radiance field is artificially generated: Using the SNR, the calibration coefficients and the leg averaged raw signal, each of them wavelength dependent, the maximum amplitude of an artificially generated white noise in the units of the radiance is determined. The product of this amplitude and the white noise is subtracted from the radiance at 850 nm. Additionally, the radiance at 850 nm is scaled to the leg averaged radiance of the considered wavelength. The artificial spectral radiances are subjected to the power spectrum analysis. The result of the analysis shows no evidence that the combination of the decreasing SNR and signal with increasing absorption intensity is the reason for the impact of gas absorption on small and large scale cloud radiative smoothing. The difference between smallest and largest slopes and scale breaks is 0.1% maximum. No correlation between absorption intensity and slopes and scale break is found in this sensitivity study.

The effect of gas absorption on cloud radiative smoothing is verified using the same cloud field as in section 5.2 and a surface albedo of A=0.4. Not only the reflectance but also the photon path length distribution is computed. Utilising the gas absorption coefficients in the $\rho\sigma\tau$-water vapour absorption band, calculated with a spectral resolution of 0.01 nm, the equivalence theorem (section 4.2) is applied to retrieve the reflectance for wavelengths between 870 and 950 nm. The wavelength dependent reflectance is convoluted with a Gauss function of FWHM=7.4 nm $\left(\sigma = \mathrm{FWHM}/\sqrt{\log\left(256\right)}\right)$, as it was found for the FUBISS instrument (section 2.1.2). The resulting reflectance, $R(x;\lambda)$, is subjected to the previously used power spectrum analysis. The noise level of the simulation seems to have no significant influence on the power spectrum analysis: If the simulated reflectances would be afflicted by noise, the noise would result in an increase of small scale energies and the corresponding spectral behaviour would show a break to smaller slopes at the smallest scales. This is not found in Figure 5.5a, at least not in scales used for interpolation and is also the case for channels affected by gas absorption (not shown).

The results are shown in Figure 5.9 which has the same setup as Figure 5.7, but for wavelength starting at 870 nm and not at 850 nm. The qualitative agreement in the course and the strength of the effect is excellent for all three parameters. Possible explanations for the difference in absolute large scale slopes are provided in the previous section. The dependence of the analysis on the spatial resolution is discussed in the next section: FUBISS's spatial resolution is 40 m while it is 10 m in case of the simulations which is probably the

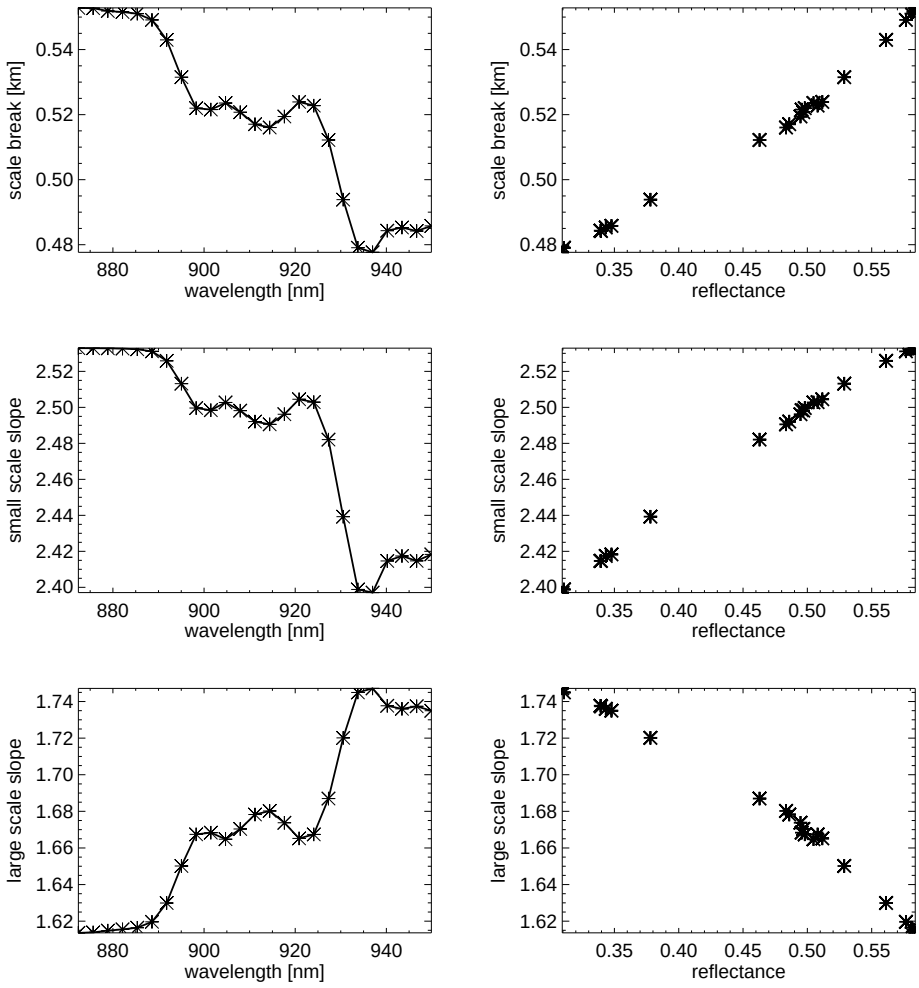

FIGURE 5.9. Scale breaks (upper panels), small scale slopes (middle panels) and large scale slopes (lower panels) versus wavelength (left panels) and versus spatial averages of simulated reflectances (right panels).

reason for the discrepancy between the absolute small scale slopes. The scale break derived from simulations is significantly larger than retrieved from observations. The reason can be found in the retrieval method, i.e. the interception of the small and large scale linear regressions. If the power spectrum is viewed, it becomes obvious that both regressions result in an overestimation of the scale break. An interpretation by eye reveals a scale break of 270 m (see Fig. 5.5a).

The argumentation, that the decrease of the small scale slope and the scale break is due to a reduction of horizontal photon transport and the likelihood of large photon paths by absorption, is justified by the following experiment: Utilising the same cloud as before, but with a reduced horizontal domain size of 5 km, ranging from 16 km to 21 km (see Figure 5.4), a total amount of 10^6 photons is inserted at the centre of the reduced cloud field (here: θ_0=0°). The reflectance is calculated for two different single scattering albedos: ω_0=1 and ω_0=0.9. In Figure 5.10 the normalised reflectances are plotted versus distance from the point of injection. Obviously the reflectance decreases faster with distance from injection, if the medium is not conservative. Additionally, the maximum range is significantly reduced.

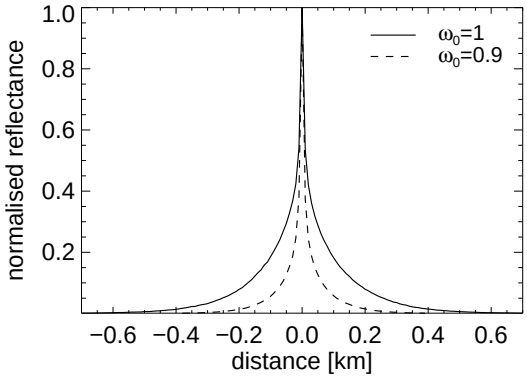

FIGURE 5.10. Normalised reflectance versus distance for two different single scattering albedos w_0. The simulation is based on the injection of photons at a single position.

In summary, absorption strongly affects large and small scale cloud radiative smoothing (the former in combination with large surface albedos). The results and conclusions are successfully verified using artificial cloud fields and RT models. A desirable extension of the analysis with RT models would be the systematic study of the relation between the scale break and the single scattering albedo. The so retrieved results may help to improve Eq. 1.8 and establish an empirical relation between the strength of the absorption and the scale break. Furthermore, the effect of liquid water absorption is interesting to study, as large interest rests on the retrieval of LWC and LWP. In this case, the verical distribution is not homogeneous, and the separation of photon path length statistics and absorption is not possible. In consequence, the equivalence theorem cannot be applied.

5.4. Difference between single and two layer cloud impacts

The spectral behaviour of two layer clouds is compared to the spectral behaviour of single layer clouds. Table 5.1 provides an overview of the observations which build the basis of this investigation. *Casi*'s nadir radiances around 620 nm are subjected to the power spectrum analysis described in section 1.2. In the single layer and two layer cloud case the solar zenith angle varied by 6° with a mean of 39° and by 8° with a mean of 38°, respectively. The impact of a varying solar zenith angle through different degrees of shadowing, cloud side illumination, and diffuse leakage through cloud sides is assumed to be small in this case (see *Loeb et al.* (1997) for intensive discussions of these effects). However, it can be expected that for small solar zenith angles diffuse leakage through cloud sides smoothes the radiation field. If the solar zenith angle is large, shadowing and cloud side illumination roughen the radiation field.

Figures 5.11a and 5.11b show the power spectrum analysis of nadir radiances at 620 nm for the single and two layer cloud case, respectively. The black dots represent the power spectrum values of the ensemble of both cloud systems. The squares result from binning, and the solid lines are the linear approximations to the binned data. The small and large scale ranges are estimated by the specifications of the majority of corresponding ranges of each of the legs of the ensemble. The small and the large scale slopes and their uncertainties are also given in Figure 5.11. Both cloud systems have almost identical small scale slopes with absolute values around 2.35. The large scale slope is much larger in the single layer cloud case (1.40 ± 0.05) than in the two layer cloud case (1.23 ± 0.04). Similar results have been found for the power spectrum analysis applied to each of the single and two layer cloud legs. The scale breaks, marked by dashed vertical lines in Figures 5.11a and 5.11b, are 412 ± 38 m and 450 ± 26 m, respectively. The uncertainties given above and in Figure

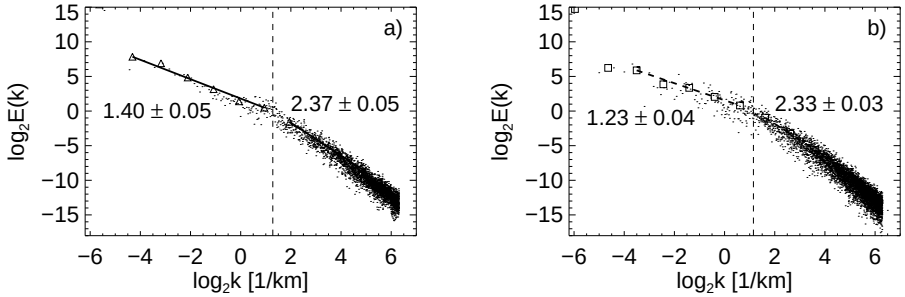

FIGURE 5.11. Ensemble power spectrum analysis of data recorded over single layer clouds on 06 and 20 September 2001 (Fig. a) and over two layer clouds on 06 and 23 September 2001 (Fig. b). The plots are based on nadir radiance measurements at 620 nm. The large and small scale slopes with corresponding uncertainties, based on five wavelength centred around 620 nm, are given. The vertical lines indicate the scale break which is given in the text.

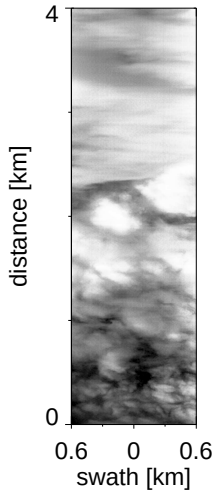

FIGURE 5.12. Enhanced *casi* image at 620 nm. The image shows the transition from a single layer (lower part) to a two layer (upper part) cloud. The data is taken from 23 September 2001 (leg 2).

5.11 are based on the procedure presented in section 1.2. Five wavelengths centred at 620 nm have been used for the uncertainty estimation. The estimates reveal that the small scale slopes and the scale breaks are not significantly separated, while they confirm that two layer cloud systems can result in an increase of large scale cloud radiative smoothing, as indicated by the decrease of the large scale slope. Note that the interpolation ranges of the large scales are chosen to minimise the difference between the large scale slopes of both cloud systems: If the bin at $\log_2 k \approx -4.5$ is excluded in the single layer cloud case and included in the two layer cloud case, the difference would be even more pronounced.

The decrease of the large scale slopes in the presence of two layer cloud systems might be explained in a similar way as the corresponding impact of the surface albedo (section 5.2). The lower layer, assumedly characterised by a large mean albedo, results in an increase of the large scale cloud radiative smoothing: optically thinner parts of the upper layer appear brighter while optically thicker parts remain unchanged. Figure 5.12 gives an

exemplary *casi* images at 620 nm (data from 23 September 2001, leg 2) which shows the transition from a single layer (lower part of the image) to a two layer cloud (upper part). The two layer cloud part appears smoother than the single layer cloud part and supports our assumption made above. In consequence, less spectral energy is needed to explain the fluctuations, and therefore, the large scale slope is smaller than for a single layer cloud. No impact on small scale cloud radiative smoothing was found for the ensemble power spectrum analysis

It is not very likely that these results are typical of all imaginable two layer cloud systems. The effect is assumed to be dependent on several circumstances: The cloud morphology (see section 5.2 and *Boers et al.*, 1988 for typical cloud diameters) is certainly an important aspect, in particular the variability of the optical properties of both layers relative to each other. If the maxima and minima of the optical thickness of both layers coincide, the effect on large scale cloud radiative smoothing is probably not observable. Additionally, the cloud morphology governs on which scales the lower layer brightens parts of the upper layer. The scale dependence is also affected by the vertical separation of both cloud layers (similar reasons as given in section 5.2). Furthermore, large scale cloud radiative smoothing by two layer clouds may not occur if the mean optical thickness of the upper layer is relatively large or if the mean optical thickness of the lower layer is relatively small. An incomplete coverage of the upper layer, as observed in both measurement cases, can cause a large variety of impacts through complex multiple scattering effects and shadowing. Note that it is not certain whether the lower layer has a coverage of 100% and if some cloud towers of the lower cloud layer penetrate the upper cloud layer.

The localisation of the scale break in the ensemble power spectrum of the single layer clouds by visual inspection is difficult since the power spectrum analysis of one of the single layer clouds has a much larger scale break than the other two single layer clouds. A different interpretation of the scale break in Figure 5.11a might result in a value of 180 m ($\log_2 k$=2.5). One can assume that the vertical separation of both cloud layers may result in a shift of the scale break to larger values.

If the results of this section are compared to the surface impact-free results presented in Figure 5.2, discrepancies between the large and small scale slopes as well the scale breaks are evident. Several factors have to be considered here. First, the FUBISS data set is longer in time than the corresponding *casi* data set, and the results given in Figure 5.11a are based on an ensemble analysis. If the analysis is redone with *casi* data received on 20 September 2001 (leg 2) and if the FUBISS data set is shortened appropriately, the large scale slopes and the scale breaks are within the overlap of their uncertainty estimates. The qualitative results given in sections 5.2 and 5.3 are not affected if the FUBISS data set is truncated to the leg length of the corresponding data set received with *casi*. The small scale slopes seem to be dependent on the sampling rate and the field of view: If only every seventh *casi* measurement is used and if the different field of views are adjusted by appropriate averaging of *casi* data, the difference between the small scale slopes is highly reduced. The conclusions are that the power spectrum analysis applied in this study depends on the section of the observed cloud field, on the pixel size, and the sampling frequency.

Min et al. (2001) came to similar conclusions. Additionally, they proposed a possible increase of horizontal photon transport due to multiple scattering between both cloud layers. This cannot be found in our results but the effect certainly depends on the vertical separation of both cloud layers and the mean optical thickness of each layer.

The quality of the presented results can be raised, if the number of cases for the ensemble analysis of power spectra is increased. Observations over well-defined single and two layer clouds (thicknesses, vertical separation, coverage) are desirable. A higher spatial resolution as well as longer flight legs, are advantageous to increase the small and large scale ranges for linear interpolation. In this way, the interpolation error can be reduced, and the identification of ranges of spectral behaviour is more trustworthy.

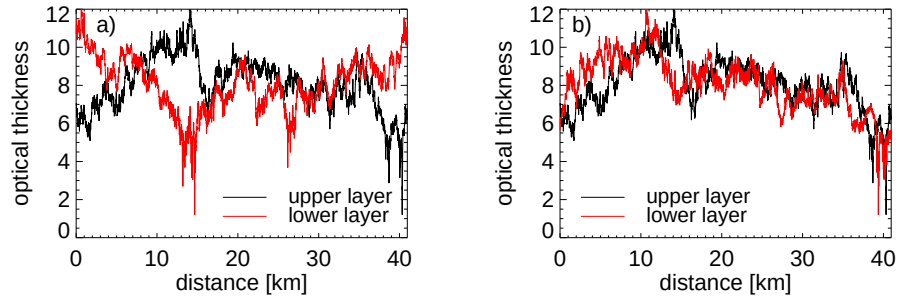

FIGURE 5.13. Optical thickness of upper (black) and lower (red) cloud layer versus distance. Figures a and b show two different scenarios based on three different surrogate cloud fields to analyse the effect of two layer clouds on cloud radiative smoothing.

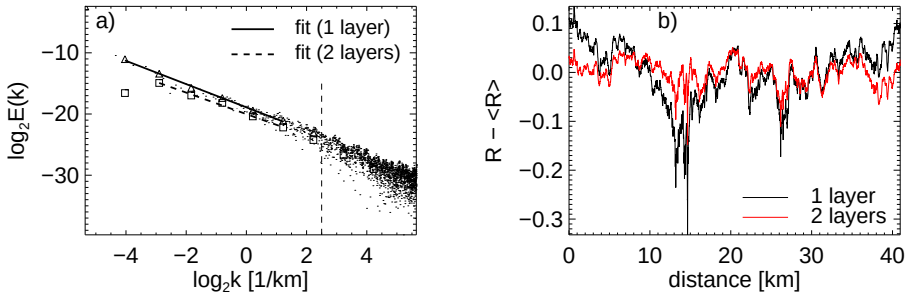

FIGURE 5.14. Two layer cloud effect on large scale cloud radiative smoothing (Fig. a), as estimated on the basis of simulated reflectances (Fig. b). The layout is similar to the layout presented in Figures 5.1 and 5.6 but here the power spectra of single and two layer clouds are compared. The dashed, thin vertical line gives the location of the scale break related to the single layer cloud. Figure b shows the mean free nadir reflectance of both systems.

The qualitative results are verified by RT simulations. The general approach is described in section 5.1, but here, two surrogate cloud fields are utilised. Both are characterised by a geometrical thickness of 200 m, vertical homogeneity, and constant cloud top and base. The lower cloud is centred around 900 m while the distance to the upper layer amounts to 400 m. In consequence, the cloud top of the two layer cloud system is at 1,500 m. The optical thicknesses of both cloud layers are illustrated in Figure 5.13, and form the basis of the simulations. The optical thickness versus horizontal distance for the upper, in black, and lower, in red, layer is shown. The single layer cloud simulations are simulated for the respective upper cloud layers. The photon number per pixel is approximately $4x10^6$. Since the focus is on the large scales, the number of photons is certainly appropriate (verify Fig. 5.14a).

First, the power spectral behaviour of simulated reflectances on the basis of the cloud field given in Figure 5.13a is investigated. The power spectrum of the single and two layer cloud is shown in Figure 5.14a. The dots present the original power spectrum of the single layer cloud, the triangles and the squares the binned power spectrum, and the solid and dashed line the linear regression of the binned data related to single and two layer cloud systems, respectively. Additionally, the dashed, thin vertical line indicates the scale

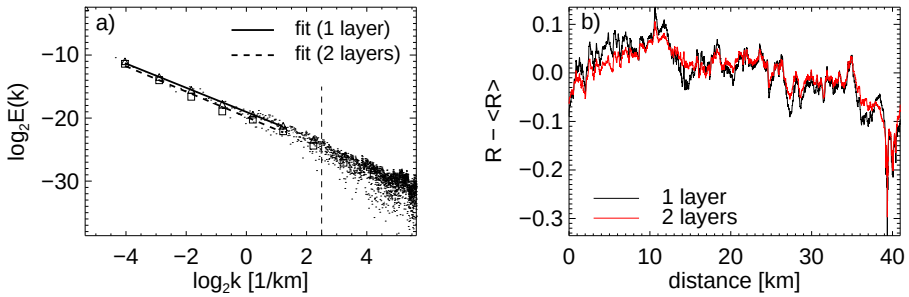

FIGURE 5.15. Two layer cloud effect on large scale cloud radiative smoothing (Fig. a), as estimated on the basis of simulated reflectances (Fig. b). The layout is similar to the layout presented in Figures 5.1 and 5.6, but here, the power spectra of single and two layer clouds are compared. The dashed, thin vertical line gives the location of the scale break related to the single layer cloud. Figure b shows the mean free nadir reflectance of both systems.

break related to the single layer cloud. The scale break is estimated by visual inspection (approximately 210 m).

Even though the low energy value at a wave number of ~2^{-4} in case of the two layer cloud is excluded from the linear regression, the less steep increase with decreasing wave number becomes obvious, if the two layer cloud case is compared to the one layer cloud case. The power spectrum analysis revealed a large scale slope of 1.90 ± 0.04 and 1.73 ± 0.03 for the one and two layer cloud system, respectively. The slopes are significantly separated by their uncertainty measures (number of channels is one) and therefore qualitatively confirm the results received from measurements. Figure 5.14b provides an explanation for the change in large scale slope. The mean free reflectance is plotted against horizontal distance for both cloud systems. Obviously $R - \langle R \rangle$ appears smoother on intermediate and large scales. The results and conclusions given during the discussion on the power spectrum behaviour of the corresponding measurements is verified.

A view on Figure 5.13a reveals, that the smoothing effect can be expected because the optical thickness of the upper layer is in anti-phase with the lower cloud layer. The question arises, if the results can be reproduced, if both clouds are not in anti-phase with each other. To test the reproducibility the minimum of $|\tau\,(\text{upper layer}) - \tau\,(\text{lower layer})\,|$ for the whole set of surrogate cloud fields, 11 in total, is determined. The corresponding optical thicknesses are given in Figure 5.13b. The power spectral behaviour of the nadir reflectance is given in Figure 5.15a. The large scale slopes with values around 1.95 are not significantly separated by their uncertainty measures. A closer look at frequencies around 2^{-1} reveal a small dip in the power spectrum of the two layer cloud case but its impact on the slope estimation is negligible. This result is confirmed by the comparison of the mean free nadir reflectances related to both cloud systems (see Fig. 5.15b). In consequence, the effect of two layer clouds on cloud radiative smoothing is not generally characterised by an increase in large scale smoothing. The occurrence of this effect depends at minimum on the relative distribution of the optical thickness of both cloud layers.

The tools presented in this work, the power spectrum analysis, the artificial cloud generation, and the RT model, allow the intensive investigation of several aspects which might affect large scale cloud radiative smoothing in the presence of two layer clouds (see also discussion related to observed radiances).